Spring 5-31-2012

fMRI assessment of ischemic stroke in humans

Rui Yuan
New Jersey Institute of Technology

Copyright Warning & Restrictions

The copyright law of the United States (Title 17, United States Code) governs the making of photocopies or other reproductions of copyrighted material.

Under certain conditions specified in the law, libraries and archives are authorized to furnish a photocopy or other reproduction. One of these specified conditions is that the photocopy or reproduction is not to be "used for any purpose other than private study, scholarship, or research." If a, user makes a request for, or later uses, a photocopy or reproduction for purposes in excess of "fair use" that user may be liable for copyright infringement,

This institution reserves the right to refuse to accept a copying order if, in its judgment, fulfillment of the order would involve violation of copyright law.

Please Note: The author retains the copyright while the New Jersey Institute of Technology reserves the right to distribute this thesis or dissertation

Printing note: If you do not wish to print this page, then select "Pages from: first page # to: last page #" on the print dialog screen

ABSTRACT

fMRI ASSESSMENT OF ISCHEMIC STROKE IN HUMANS

By

Rui Yuan

Cerebral ischemia, or brain ischemia is a kind of stroke where the blood flow is insufficient to the metabolic demand of brain. The lack of oxygen supply will directly lead to the death of brain tissue. There are two major injury regions: the infarct and penumbra. Mostly, since the infarct regions became dead tissues rapidly after stroke, there is a tiny possibility to rescue them in time. But penumbra parts are different. Tissues there will be viable for hours after ischemia. Hence, both theoretically and practically, it is possible to salvage those cells in the penumbra region. Diffusion weighted image (DWI) is a widely used and robust tool to detect ischemia lesions. Unfortunately, DWI can only quickly and accurately detect the location of lesions, however, it cannot distinguish the infarct and penumbra, which is vital to act on further treatment. The main goal of this study is that the functional MRI data can be used to obtain both structural and functional information about lesions in stroke patients.

It was hypothesized that the lack of oxygen supply might be directly caused by lower level rate of blood flow, which can be traced by blood-oxygen-level-dependent (BOLD) signal. Hence, through working on the functional MRI data, it is possible to find the difference between infarct and penumbra.

Through different kinds of algorithms, the functional MRI data can find certain levels of difference between the ischemic lesions and normal tissues.

fMRI ASSESSMENT OF ISCHEMIC STROKE IN HUMANS

by
Rui Yuan

A Thesis
Submitted to the Faculty of
New Jersey Institute of Technology
in Partial Fulfillment of the Requirements for the Degree of
Master of Science in Bioelectronics

Department of Electrical and Computer Engineering

May 2012

.

APPROVAL PAGE

fMRI ASSESSMENT OF ISCHEMIC STROKE IN HUMANS

Rui Yuan

Dr. Durgamadhab Misra, Dissertation Co-Advisor — Date
Professor of Electrical and Computer Engineering, NJIT

Dr. Bharat Biswal, Dissertation Co-Advisor — Date
Associate Professor, Department of Radiology, UMDNJ

Dr. Yun Qin Shi, Committee Member — Date
Professor of Electrical and Computer Engineering, NJIT

BIOGRAPHICAL SKETCH

Author: Rui Yuan

Degree: Master of Science

Date: May 2012

Undergraduate and Graduate Education:

- Master of Science in Bio-Electronic Engineering,
  New Jersey Institute of Technology, Newark, New Jersey, 2012

- Bachelor of Engineering in Electrical Engineering,
  Chengdu Normal University, Chengdu, P. R. China, 2010

Major: Bio-Electronic Engineering

To my parents, who gave me a love of life.

To my grandfather, who taught me that a good life is one inspired by love and guided by knowledge.

.

Three passions, simple but overwhelmingly strong, have governed my life: the longing for love, the search for knowledge, and unbearable pity for the suffering of mankind. These passions, like great winds, have blown me hither and thither, in a wayward course, over a deep ocean of anguish, reaching to the very verge of despair.

-Bertrand Russell

ACKNOWLEDGMENT

I would foremost like to express my earnest gratitude to my research co-advisor, Dr. Bharat B. Biswal, for his patient and inspiring guidance throughout this research work. I would also like to thank my research co-advisor, Dr. Durgamadhab Misra, for his constant support, guidance and valuable suggestions throughout this research study. I am also indebted to my committee member Dr. Yun Qing Shi, for his valuable inputs during the review of this research work.

TABLE OF CONTENTS

TABLE OF CONTENTS

(Continued)

LIST OF TABLES

LIST OF FIGURES

CHAPTER 1

INTRODUCTION

1.1 Overview

According to the US health statistics, approximately 800,000 people suffer from stroke and other forms of cerebrovascular accidents every year. It is currently one of the three leading causes of death in the United States. Although stroke affects people across a wide age span, the stroke incurred can be categorized into 2 main types: ischemic stroke and hemorrhagic stroke. Ischemic stroke is the most common form of stroke and accounts for about 85% of all stroke cases. The ischemic stroke is typically caused by insufficient blood flow (and consequently oxygen and nutrients) to the brain. This reduction in blood flow causes death of brain tissue. Based upon the location of the ischemic stroke may impair a patient's vision language, memory and motor skills. If not treated immediate, these dysfunctions tend to remain for the rest of the patient's lifetime. Thus, rapidly and efficiently detecting brain infarction remains critical for accurate treatment and assessment of rehabilitation. The second type of stroke is called hemorrhagic stroke and currently accounts for about 15% of the strokes. This is caused by the leakage of blood flow in the brain. (Hinkle et al., 2007; Jones et al., 1981)

The progression from normal cerebral blood flow (about 70 mL/100g/min) to ischemia occurs in three distinct stages. During the first stage, the cerebral blood flow drops below 60 mL/100g/min. At this stage a substantial number of neurons are still active. The second stage, or called the penumbra phases, the blood flow keeps on dropping and reaches about 20 mL/100g/min. During this stage, there is significantly less electrical communication between neurons. During the third or most critical phase, when

blood flow goes below 10 to 15 mL/100g/min, it will result in ischemic cascade. Importantly, through this stage, all the effect that ischemic cascade make will be irreversible. Further, it will mostly lead to cell death (apoptosis) (Jones et al., 1981).

Functional disruption caused by ischemia results in structural regions. There are two main regions inside ischemic lesions. The core region, named "infarct", is the core representing the severe ischemic region where irreversible tissue destruction has occurred. The infarct regions are surrounded by the penumbra. The penumbra region refers to the region at the rim of infarct and between normal tissue and infarct. In this region, Cells are still viable in several hours after stroke, which can be treatable. Thus, immediately after occurrence (or suspicion) of stroke, it is critical that stroke is diagnosed correctly and accurately since this can then determine the treatment strategies and ultimately patient outcome.

In order to detect and visualize lesions for the further treatment, medical imaging has played a crucial role in stroke research. Due to its high spatial resolution in addition to its non-invasiveness, magnetic resonance image (MRI) is increasingly being used as an essential diagnostic tool to study stroke.

In addition to obtaining high spatial resolution images using MRI, Dr Denise Le Bihan (Bihan et al., 1986), first used diffusion weighted MRI image (DWI), to demonstrate it as a robust way to detect the infarct in the brain. The principle of DWI depends on the "Brownian motion" of water in the brain tissue. Water molecules are in constant motion, and the rate of movement or diffusion depends on various physical characteristics including particle size, viscosity of the liquid. In biological tissues, diffusion is not truly random because tissue has structure. With the respect of brain,

waters flow through membrane of neuron and neuron cells. Hence, through the diffusion weighted imaging, one can quantify diffusion with high spatial resolution on voxel wise basis. In clinical cases including brain tumors or stroke that cause lesions, have a differential effect on the activation of neuron cells, which ultimately affect the water diffusion. Thus, DWI is addition to taking less time to reveal the infarct compared with conventional T1 or T2-weighted MRI images (Warach et al., 1992). Moreover, every voxel in the brain also provide a quantitative information about the rate of water diffusion. Hence, in this study, DWI (diffusion weighted image) was used as the method of choice for lesion detection.

However, one of the disadvantages of DWI is that it is very difficult to distinguish between the infarct and the penumbra. Further, in most cases, the acquisition of DWI images can take up to 10 minutes during which the subjects have to lie still without moving their body. From a clinical point of view, the penumbra part has more practical meaning than infarct, since with treatment they can be revived.

In recent years, advances in hardware and software have resulted in the acquisition of MRI images at a fast rate. Using functional MRI (fMRI), subjects perform sensorimotor, memory or cognitive tasks. These tasks are presented in a periodic "ON/OFF" paradigm, where short duration of tasks are alternated with durations of rest periods. A variety of statistical procedures including t-test, correlation, or F-test is then used to identify the location and quantify the signal changes in the brain.

In recent years, resting state fMRI, scanning subjects, during the absence of any specific tasks, i.e., while subjects are at rest, has emerged as a viable alternative to task activation paradigm. During resting state scans, the subjects simply have to lie down and

relax, with their eyes closed (or eyes open). Currently, there are various methods being developed to analyze resting state data. Most of them are focused on the connectivity patterns between distinct regions of the brain using both on time and frequency domain signal analysis (James et al., 2002; Wards et al., 2003).

In this study, the focus is to investigate the temporal and frequency structure of the resting state fMRI signal in patients with ischemic stroke. Although fMRI has a lower spatial resolution than MRI, it can provide functional information about the dynamics of the brain in addition to structural information. Further, because patients with ischemia stroke might not be able to perform any task, thus it is appropriate to scan those patients at resting state.

1.2 Objective

The goal of this study is focused on using signal processing and statistic methodologies to detect lesions in stroke patients. In this study, we hypothesized that physiological information from functional MRI data can be used to obtain both structural and functional information about lesions in stroke patients.

1.3 Background Research

With the development of technology, a number of medical imaging modalities including MRI, CT, and PET have been used to detect lesions in the brain.(Lutsep et at.,1997; Van et al., 1998) Compared with these images, diffusion weighted image has several great advantages and has evolved into a robust tool to detect lesions caused by ischemic stroke. First, diffusion image takes less time to generate images than other conventional MR images. In most case, five to seven minutes are adequate for diffusion imaging. Secondly,

the accuracy of DWI is higher than CT or T2 image. Third, it detects lesion at early onset of stroke (within an hour of stroke), while lesions are invisible for several hours using conventional MRI imaging.

The fundaments of DWI are largely based on a microscopic phenomenon called Brownian motion. In the brain, the water molecules can roam freely or randomly diffuse across cell membrane and capillaries. The movement of the water diffusion is affected by its temperature, the kinetic energy of molecules. The diffusion coefficient of water is 0.003mm^2/sec at body temperature. But water diffuses restrictedly across tissues, because tissue has microstructures. Thus, apparent diffusion coefficient (ADC) is used to describe the movement of water in tissue. Its value is smaller than the pure water diffusion coefficient. It will decrease while the time of measurement lasts. Because as time goes, more and more water molecules will occur restriction. The signal intensity of diffusion image is calculated by the equation:

$$\mathrm{ADC} = e^{-D \cdot b} \cdot e^{-TE/T2} \tag{1.1}$$

Where, b is diffusion sensitivity, D is water diffusion, and TE is echo time and T2 is relaxation time. As this equation shows, ADC map might provide a more accurate image to detect lesion than DWI as it describe the diffusion restriction without the influence of T2 signal. In the case of ischemia, the signal intensity is affected by the cytotoxic edema, which cause large amount of water fluxing into cell. This kind of shift of water from extracellular to intracellular will definitely results in signal intensities increasing. By comparing with normal diffusion intensity, those increased intensities can demonstrate the location of lesions. (Chen et al., 2006) In this study, diffusion weighted image (DWI) is used as the lesion reference.

A large number of researchers have showing using fMRI, alteration in the resting state network properties or brain reorganization after stroke (James et al., 2002; Wards et al., 2003). However, to the best of our knowledge, there has been no research performed to locate and characterize lesions following stroke. Thus this study is the first time to detect lesion by using spatio-temporal properties of fMRI signal.

1.4 Outline

This thesis is divided into three parts. Chapter 2 presents a brief overview of ischemic stroke. It briefly introduces the basic concepts about how ischemia occurs and how it progresses. In chapter 3, Nuclear magnetic Resonance, Magnetic Resonance Imaging, Functional Magnetic Resonance Imaging and MRI instrumentation are introduced. Chapter 4 explains the preprocessing steps developed and used in this project. Chapter 5 describes processing strategies for detecting lesions on fMRI, which includes the main signal processing method, and statistics analysis. In chapter 6, the result of the lesion detection and further steps to distinguish infarct and penumbra are discussed.

CHAPTER 2

THE PATHOPHYSIOLOGY OF ISCHEMIC STROKE

2.1 Introduction

According to the medical definition, stroke, or cerebrovascular accident is the sudden death of brain cells at certain regions of a brain due to the lack of oxygen and glucose, which is caused by an inadequate blood flow (Goldstein et al., 1989). There are two main types of stroke, ischemic and hemorrhagic, which accounts 85% and 15% all strokes respectively (Hickey et al., 2003). Because of the fact that brain cells do not store glucose, after stroke occurs, the main energy sources are cut and brain cells are incapable of performing anaerobic processes. According to the rate of onset and duration, collateral circulation, the stroke can result in permanent neurologic damage, disability, or even death since ischemic cascade is a rapid process.

There are many etiologic mechanisms to explain the pathway of ischemic stroke from the molecule level to the system level. (Matthew et al., 2009) In general, the mechanism of ischemic stroke can be summarized by three main types: thrombosis, embolic stroke and global ischemia stroke. In some cases, systemic congestion and venous congestion are also regarded as distinguished types. Rarely, the use of cocaine (Blank et al., 1996) and antiphospholipid antibodies coagulation can also cause ischemic stroke.

Thrombosis is main reason for nearly 50 percent of all strokes. The clot developed in extracranial and intracranial arteries will travel around within blood flows. When these clots reach to a narrow spot and cut a blood flow, the stroke occurs. According to the location of forming, the thrombosis can be divided into additional types: large-vessel

thrombosis and small-vessel thrombosis. For the large-vessel thrombosis, the blockage is formed at the large cerebral arteries. Compared with the large-vessel thrombosis, the small vessel thrombosis refers to block clots which are formed at smaller and deeper location within arteries. The formation of microscopic thrombi is a complicated phenomenon. Basically, the forming is usually started around the diseased or damaged cerebral arteries, where endothelial injury causes a roughened surface covered by aggregated plaques. When these plaques coagulate, the thrombus develops.

Moreover, clots can also form at other place even outside brain and flow into cerebral arteries. The stroke caused by this kind of clot is called embolic stroke. Mostly, these clots are developed from the heart. The common sources are the left-side cardiac chambers and large arteries. The clot or emboli can flow through the bloodstream until it reaches to a narrow spot and lodges. Unlike thrombosis, the emboli consist of blood and fat. Commonly, long bone and cardiac surgeries, tooth loss can cause the forming of emboli (Joshipura, et al., 2003).

Although it is uncommon, in some rare case, the adequately low blood pressure can decrease the oxygen and glucose supply and cause an ischemic stroke. This kind of stroke is called hypotensive stroke or global ischemia stroke (Goetz et al., 1999). Mostly, the largely decreased blood pressure might be caused by cardiac pump failure, a severe infection, over-treated high blood pressure.

After blocked or largely decreased blood flow in the brain tissue, the plunged process of blood supply will lead to the ischemic cascade. The ischemic cascade is a series of biologic and chemistry processes, such as excitotoxicity, reperfusion injury, cerebral edema (Hinkle et al., 2007). Once started, even supplying blood flows to those

regions again, the process will not stop. In general, the result of ischemic cascade is the apoptosis, a regulated cell death.

2.2 Detection of Infarct

Currently, several medical imaging techniques could detect lesions caused by ischemic stroke, such as CT, T2 weighted image, diffusion weighted image, apparent diffusion coefficient. As the stroke mechanism described above, the brain ischemia causes edema, which is highly related with water diffusion. Compared with CT or T2 weighted MR imaging, which have less than 50 percent of lesion detection in the first 6 hours of stroke, diffusion weighted imaging has a high sensitivity which ranges from 90% to 100% (Maarten et al., 2001; Mullins et al., 2002).

Hence, DWI is also called “the stroke sequence”. Its imaging contrast is mainly based on the Brownian motion of extracellular water. Moreover, its acquisition time is relatively short, and no additional contrast is required. In this study, Diffusion weighted image is used as a reference image .Here is an example of diffusion weighted images:

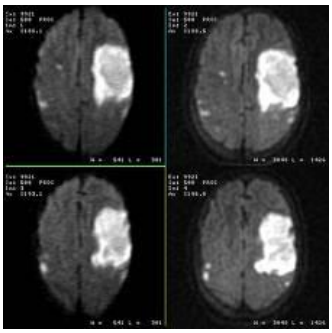

Figure 2.1 Diffusion weighted image sample
Source: http://www3.americanradiology.com, accessed on May 14, 2012

The bright part in the image indicated the lesions. Due to its ineffectiveness at distinguishing the infarct and penumbra, the bright region may include reversible tissue.

Except the diffusion weighted imaging, there is another way called apparent

diffusion coefficient (ADC) to present the water diffusion images (Bihan et al., 1986). Basically, ADC is generated by two diffusion weighted images, and intensities of ADC images are calculated voxel by voxel from DWI images (Woodhams et al., 2011). The equation is:

$$\text{ADC value} = -\ln(Sdw/Sse)/b \quad (2.1)$$

The Sdw is the attenuated spin-echo signal and Sse is the full spin-echo signal without diffusion attenuation. Thus, a low ADC value refers to the high diffusion intensity. Here is an example of comparison between ADC and DWI:

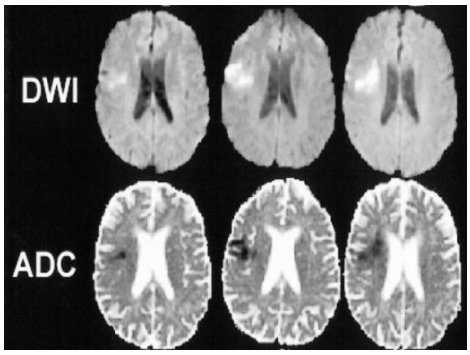

Figure 2.2 Comparisons of ADC and DWI

Source: Maarten G. Lansberga, Vincent N. Thijsa, Michael W. O'Briena, Juan O. Alia, Alex J. de Crespignya. (2001). Evolution of Apparent Diffusion Coefficient, Diffusion-weighted, and T2-weighted Signal Intensity of Acute Stroke. AJNR, 22, 637-644

CHAPTER 3

FUNDAMENTALS OF MAGNETIC RESONANCE IMAGING

For the past two decades, functional magnetic resonance imaging (fMRI) has been widely used in the field of neuroscience and cognitive science. The fMRI is based on magnetic resonance image (MRI). Before the era of MRI, medical images were primarily based on the x-rays, computed tomography, and positron emission tomography. However, all these medical imaging techniques are ionizing radiation based and have different contrast mechanisms. They definitely would damage tissues at a certain level and cannot been utilized to show the dynamic changes of the brain without injecting any labeled chemicals. This chapter describes the basic concepts and mechanism of the MRI imaging.

3.1 Nuclear Magnetic Resonance Physics

The principle of how magnetic resonance imaging works is largely built on the phenomenon of the rotation and emitted energy of nuclei of atoms in strong magnetic fields. The atom consists of nuclei and electrons. The nucleus can be divided into protons and neutrons. The neutrons do not have any charge, but the protons have positive charges. Basically, the atoms have a balanced charge, which means that the nuclei and electrons have an equal amount of charges. Due to its simple structure and abundance in human body, the hydrogen nucleus is typically used as the MR active nucleus. The hydrogen nucleus consists of a single proton, so it can provide a relatively stable magnetic moment. According to the quantum mechanical properties, the nucleus, which has a positive charge and a consistently spinning proton, also have a small magnetic moment.

Hence, if hydrogen nuclei were placed into a static and strong magnetic field, many hydrogen nuclei will be energetically forced to align with the applied magnetic field. Since these hydrogen protons stand at two different states, low or high energy, the magnetic orientation can be quantified (0 or 1). The low energy nuclei will be parallel to the external magnetic field. On the contrary, the high energy nuclei can be identified as anti-parallel direction. At the equilibrium, there will be slightly more low energy nuclei than high level energy nuclei and all nucleuses are aligned along the external magnetic field, it is the time that they reach to the equilibrium. The difference between the number of the high and low energy nuclei is the longitudinal magnetization. The magnetized process can be described by the equation:

$$M(t) = M_0 \cdot (1 - e^{-t/T1}) \tag{3.1}$$

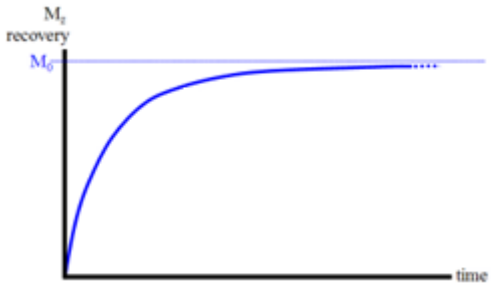

Figure 3.1 The magnetized process

The M(t) is the magnetization along the z direction as the B0 field. M_0 is the strength of the magnetic field. Since B0 is constant, the M_0 is fixed. "t" is the time of recovery. In the exponential process, T1 is a specified constant time when the magnetization recovers to the 63% of equilibrium magnetization. When a constant magnetic field is applied to the nucleus, the magnetic moment of the proton will start to spin or precession about the magnetic field because of the influence of B0. Since all the

protons have the same mass and charges, they process at the same rate in the same external field. The relationship between the precession and magnetic field is known as the Larmor relation:

$$f=ϒB \tag{3.2}$$

In this equation, f stands for the frequency of rotation (the number of rotations per second), B represents the strength of the external magnetic field. "ϒ" is the Larmor constant, which also is called as gyromagnetic ratio or magnetogyric ratio. For the hydrogen nucleus, this Larmor constant is 42.58MHZ/T.

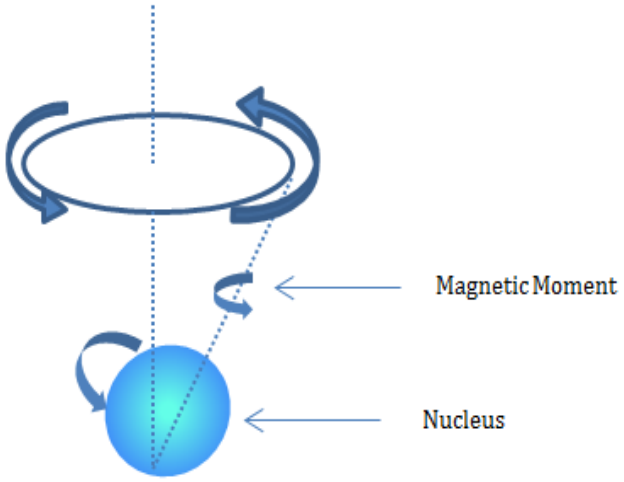

Figure 3.2 Precession of a nucleus under the effect of the Magnetic Field B0

The precession is vital for MRI imaging, because it can be utilized to construct MR images.

Then another magnetic field B1 is applied to the nuclei, which is along the transverse plane (x or y plane). B1 is not a constant magnetic field as B0, indeed it rotating around longitudinal axis in the x-y plane. The B1 magnetic field can flip the net magnetization 90 degrees from z plane into x-y plane, which means totally demagnetize

nuclei. After the longitudinal magnetization vector moves to the transverse magnetization vector, the transverse magnetization vector rotates or precession around the transverse magnetization.

Resonance is the physical phenomenon in which objects tend to oscillate at the maximum amplitude at a specific frequency. When a nucleus is in a magnetic field which oscillates with a frequency near the nucleus's Larmor frequency, the nucleus can gain energy from it and start the resonance. The frequency of a nucleus resonance belongs to the radio frequency band. Indeed, in order to make nuclei smoothly precession at the transverse plane, the nuclei are supposed to be at the resonance state, which means B1 should rotate at the nuclei' Larmor frequency. In the MRI field, the method of triggering resonance by radio frequency (RF) pulses is called excitation.

Since the transverse magnetic field consists of tons of protons, if the B1 is turned off, the MR signal will quickly decay after being created because there is no perfect homogeneous magnet and the nucleus magnetic field is easily disturbed. The process of MR signal decay is described mathematically as:

$$\mathrm{Mxy(t)} = \mathrm{M_0} \cdot e^{-t/T2} \tag{3.3}$$

T2 is a parameter that represents how fast the transverse magnetic field decays. M_0 is the equilibrium magnetization.

According to Faraday's law, if a conductive loop is in a time-varying magnetic field, a currency will be induced immediately in the conductive loop. Thus, the rotating magnetic field B1which created by RF pulses can generate a specific currency by standard antennas as the magnetic resonance signal. The amplitude and frequency of the detected currency is depended on the amount of nuclei and how the magnetic field varies.

Since the radio signal does not provide accurate information about location, it needs further magnetic fields to locate positions. Therefore, the second magnetic fields with different gradients can be applied on the first magnetic fields. This superimposed magnetic field can cause predictable variations of magnetic field along three axes. Therefore, through detecting the MR signal's frequency, positions of voxels are determined in the three dimension origins. Then through calculating the amplitudes of the MR signals at a specific frequency, image is created by filling those values to specific voxels.

3.2 Image Weighting and Contrast

Compared with other medical imaging techniques, such as CT, MRI can provide an excellent contrast to distinguish different soft tissues. For images, contrast means the difference between neighboring voxels. The bigger their difference, the bigger the contrast the image has. For MRI images, the high intensity or signal corresponds to large transverse magnetization. The bright parts of images are mostly caused by the large transverse magnetization received by RF coils. On the contrary, the dark areas are caused by low transverse magnetization, which means that the nuclei are slowly magnetized at that area. Due to the amount of hydrogen, fat and water are at the poles of contrast. There are three kinds of mechanism to build contrast, T1 recovery, T2 decay and proton density.

T1 recovery is the consequence of nuclei releasing energy to the environment and the magnetic moment flipping back to relax, anti-parallel along the longitudinal plane. Different tissues have different rates of recovery to equilibrium.

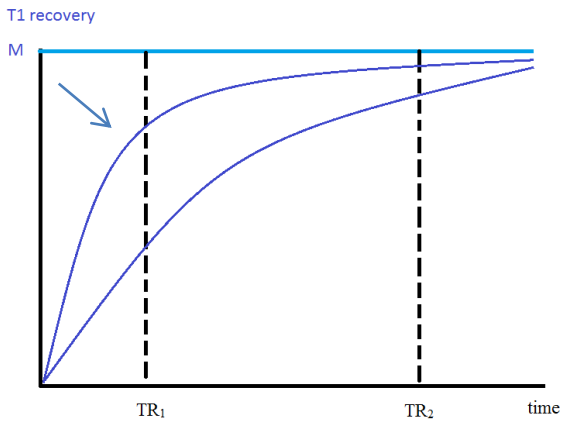

Figure 3.3 T1 recovery curves

The difference of fat and water predominantly determine the contrast of the T1 image. Because fat (the one with arrow) and water are two extreme intensities in the image, all others are intermediate. For the T1 image, a shorter relaxation time (TR) and a shorter echo delay time (TE) should be used to get the contrast for different tissues. Just like the Figure 3.3 shows, TR_1 is an appropriate time to make a contrast since neither the fat nor the water gets to the equilibrium. At the time point of TR_2, the fat have already reached at the equilibrium status, which means some of the tissue similar to fat might reach to equilibrium too. If so, the contrast might fail to distinguish the difference among those tissues.

For the T2 weighted image, the contrast in the MR signal is generated mainly by the loss of transverse magnetization. The nuclei in the tissue interact with neighbors, and cause the decay of the transverse magnetization. The rate of decay is an exponential process similar to T1 through the decay of signal here.

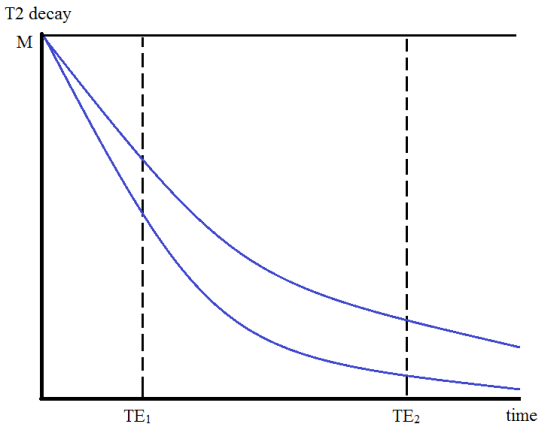

Figure 3.4 T2 decay curves

The echo delay time (TE) is regarded as the dominant parameter for the contrast of T2 image. As the figure shows, TE has to be long enough to have a good contrast, such as TE_2. If the TE is chosen at the time TE_1, the contrast between fat and water is too small and it is difficult to distinguish other tissues in that range.

The proton density image describes the density of protons per voxel in the scanned objects. In order to have the proton density contrast, the T1 and T2 effects have to be minimal. Therefore, the way to choose the TR is to wait nucleus of both water and fat recovering to equilibrium. As for TE, it has to be very short before the water and fat decaying.

3.3 MRI Instrumentation

The MRI contains four components: the nuclear alignment, the radio frequency excitation, the spatial encoding and the imaging formation. In order to complete all these functions, specific apparatuses are required. First, a magnet is mandatory. It can force all the nuclei into alignment. Then, gradient coils, which determine the spatial positions of MR signals. Third, RF coils are used to exit and perturb the nuclei.

3.3.1 The Main Field

The main field is the vital component for the alignment. It has to provide a very strong and static magnetic field B0. In order to create an exceptionally precise and homogeneous magnetic field, shim coils should be putted between the gradient coils and magnet coils. Currently, the MRI scanners utilize superconducting electromagnets to generate magnetic fields, which range from 0.5 to 9 tesla for humans and even higher for the animals.

3.3.2 Gradient Coils and Amplifiers

Since the gradient coils generate the magnetic field for spatial encoding, the most significant feature of the gradient coil is its speed. It provides each line in the space with an increasing Larmor frequency in three directions. Through these changing frequencies, the currency is collected for each slice .If the speed of the magnetic field change can be increased, the total time spent on the imaging can be dramatically decreased.

3.3.3 RF Coils and RF Coil Arrays

The radio frequency coils transmit and receive the electromagnetic energy from protons at the Lamor frequency. They generate radio frequency pulses to force nuclei to flip their magnetization vectors from z plane to the x-y plane and from a low energy level to a high energy level. RF coils are the key point for the quality of the MRI scan. In general, there are two ways to improve the quality of images by modifying the RF coils: first, the easiest way to reduce noise is to make the RF coils as small as possible. Undoubtedly, the shorter the distance, the less noise received from the object in the scanner. Second, using arrays of coils is a progressive way to improve image quality. They can collect different parts of images at the same time, which can largely decrease the imaging time and reduce

the changes conducted by motion. Also the homogeneity of the RF coils is not as strict as the main field, because the inhomogeneity can be fixed in the process of reconstruction.

3.4 Functional Magnetic Resonance Imaging

Originated from the MRI, fMRI provide another scope of view of brain. MRI mostly focused on the structural anatomy, but fMRI focused more on the physiology dynamics. fMRI is a versatile and non-invasive method to explore the brain function and neural activities. fMRI is based on blood oxygen level dependent (BOLD) contrast, which has discovered by Seiji Ogawa (Ogawa et al. 1990a,b). Basically, it is specialized to measures the neural activities in the brain or spinal cord of humans or animals, but also used to study the dynamics of neural networks across different spatial and temporal scales. Indeed, what fMRI measured directly is not neural activities but haemodynamic changes, such as blood volume, blood flow changes.

3.4.1 Blood Oxygen Level Dependent (BOLD) Signal

As mentioned previously, the Blood Oxygen Level Dependent signal, as its name, is based on the oxygen and deoxyhemoglobin changes. By the BOLD signal contrast, fMRI can provide positron emission tomography-like images, which can depict detailed information on neural activity. The relationship between the neural activities and BOLD signal has been explored for years. The fundamental principles of the relationship are fairly clear. When the neuron activities occur, the blood flood increases gradually to supply oxygen and glucoses. Interestingly, the amount of oxygen that the blood flow supplied is not matched with the amount of oxygen that neurons consume. Even at present, the mechanism of this mismatch is unclear.

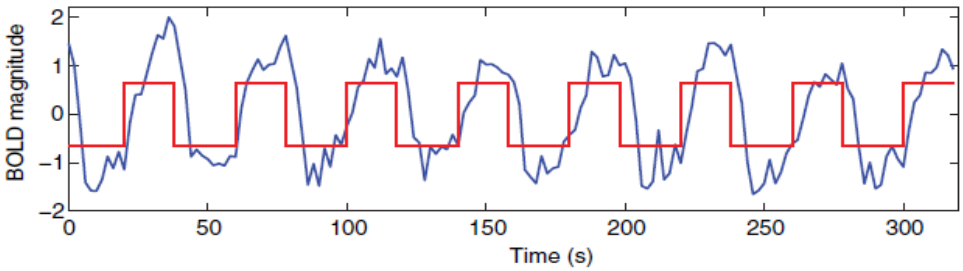

Figure 3.5 BOLD signal and simulator input series

Source: Poldrack RA, Mumford JA, Nichols TE. (2011). Handbook of fMRI data analysis. New York, Cambridge University Press.Poldrack et al., 2011

It is much easier to explain the mechanism of BOLD signal on the active voxel. Commonly, for a linear system, the best way to understand its mechanism is to find its impulse response function. In order to find the response function, a stimulus series are sent to the system as input. Comparing the input and output of the system, the system response can be describes. For the BOLD signal, the way to describe its mechanism is very similar to the linear system model since there is a consensus that HRF has a linear time invariant property (Poldrack et al., 2011). After the neuron stimulus, the system response occurs. Usually, this system response is called the hemodynamic response. As the figure 3.5 shows that, the red line is the input time series, and the blue line is the hemodynamic responses. There are lots of previous studies on the hemodynamic response fuction (HRF). Through deconvolution models, a doubled gamma function can be found to describe the HRF (Fristion et al., 1998; Lange et al., 1997). However, as many evidences show, HRF cannot be described by a signal or several models, because hemodynamic responses may vary between individuals, even between regions in one brain. However, if a complex model is made with more flexibility, such as the canonical HRF plus derivative model and finite impulse response models, the estimate of hemodynamic responses may have more bias.

Although BOLD signals are generally based on the hemodynamic response and highly correlated with neural activities, BOLD signals are also affected by various physiological and non-physiological sources such as respiration, heart-rate, and noise from scanner hardware (Dagli et al., 1999; Wise et al., 2004; Jo et al., 2010).

3.4.2 Resting-state fMRI

Mostly, fMRI researches are based on certain task settings by triggering specific brain regions. By detecting the BOLD signals under these task settings, the mechanism of brain function network and model are observed. Undoubtedly, the underlying logic of task settings is simple that the brain activities would represent how neural network works to respond the external stimulus.

In the nearly 15 years after the invention of fMRI, researchers started to explore the meaning of the resting state fMRI. Compared with normal task driven fMRI experiment, the resting state fMRI refers to the status of the scanned subjects. During the fMRI scanning, all those subjects were instructed to relax, keep still, and not think about anything. The first resting state fMRI study was performed by Biswal and colleagues (Biswal et al., 1995). They found that the synchronous low frequency fluctuation (LFF) ranges from 0.01 to 0.08 has a high correlation between left and right motor cortex regions at resting state which were coincident with BOLD motor activation map just like Figure 3.6 demonstrated. (Biswal et al., 1995, 2010; Raichle et al.,2001; Greicius et al., 2004; Fox et al., 2005; Damoiseaux et al.,2006; Fox and Raichle, 2007; Roy et al., 2009). Then studies have shown there are same kinds of correlations in auditory, visual cortex (Cordes et al., 2001; Lowe et al., 1998; Kiviniemi et al., 2004). Those discoveries broke a

common bias that the resting state fMRI cannot demonstrate any meaningful result from some nearly silent small fluctuations.

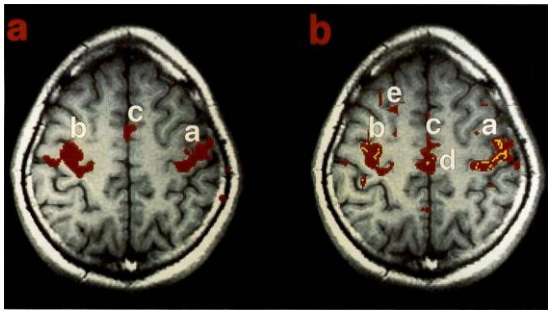

Figure 3.6 (Left) FMRI task-activation response to bilateral left and right finger movement (Right) Resting state fluctuation response

Source: Biswal, B., Yetkin, F.Z., Haughton, V.M., Hyde, J.S., (1995). Functional connectivity in the motor cortex of resting human brain using echo-planar MRI. Magn Reson Med. 34, 537–541.

Except those fundamental neural network studies, resting-state fMRI has also been used on clinical studies, such as motor cortices in multiple sclerosis (Lowe et al., 2002), Alzheimer disease (AD) (Li et al., 2002; Greicius et al., 2004), depression (Anand et al., 2005). In the stroke field, there have been many studies based on fMRI (Carey et al., 2002) (Ward et al., 2003 a,b). But mostly, all those studies are in the task settings. Moreover, studies based on resting state fMRI focused more on the brain function changes and brain function recovery than on structural information of lesions. As mentioned in the chapter 2, diffusion weighted imaging provides an accurate and fast way to detect lesions. It is redundant to use fMRI, a time-cast and lower resolution way to locate lesions. However, the weakness of diffusion weighted image on distinguishing the infarct and penumbra might be complemented by fMRI study. The way of the BOLD signal reacts at the infarct and penumbra regions needs to be explored.

CHAPTER 4

DATA ACQUISITION AND ANALYSIS

Just like a film made in a studio needs to be edited and processed before being showed in theaters, fMRI data also needs preprocessing operations to prepare the data for analysis. In the majority of cases, preprocessing plays an important and major role in the whole analysis. Because there will be some potential artifacts and unwanted noises in the acquired data, which are caused by the MRI scanner itself or by the head motions of scanned individuals, some steps of preprocessing are meant to detect and remove these artifacts or eliminate some of the effect of artifacts in datasets. This chapter specifically describes the data preprocessing and data analysis methods used in this study.

4.1 Preprocessing Steps

The preprocessing is the first and paramount step for the analysis. Each of the steps in the preprocessing is to improve the quality of the dataset. It is also always necessary to check the output of each steps of preprocessing. Occasionally, there are some very "bad" datasets, which have lots of head motion and ghosting that the preprocessing operation cannot fix at all. Then leaving the dataset alone would be a better choice. All the fMRI data in this experiment were preprocessed by using AFNI (Cox et al 1996). Generally, there is a step before the motion correction, named the distortion correction, which is mostly mentioned in preprocessing steps to remove the effect of the inhomogeneity of magnetic field. But in order to avoid any artifacts which might be generated by operations of the distortion correction, distortion correction is not used in this study. The preprocessing flow is shown by the figure 4.1.

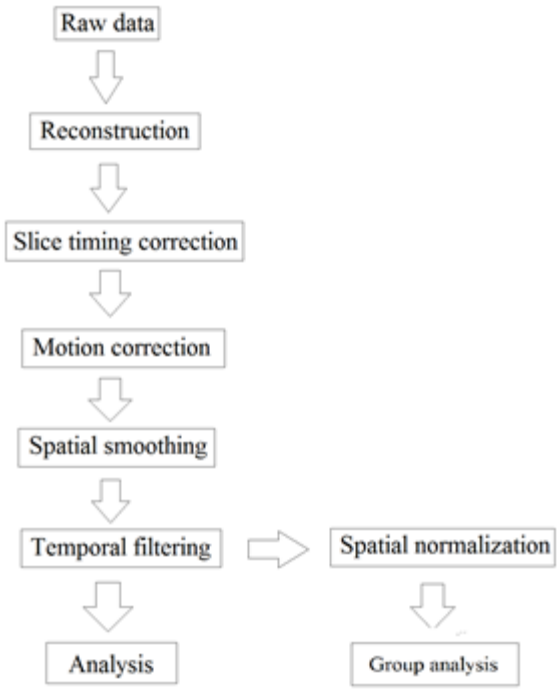

Figure 4.1 The preprocessing steps.

4.1.1 Reconstruction Datasets

Usually, the images obtained from MR scanners are in the DICOM format. Indeed, DICOM stands for "Digital Imaging and Communications in Medicine," which is a medical imaging standard. Images in this format are not just plain figures, but also include all sort of information about the patients. Thus, basically, the DICOM format files are more like a patient profile with images rather than simple medical images, such as NIFTI file.

In order to work further on those images, it is necessary to convert the DICOM files into NIFTI files. Compared with DICOM files, images in NIFTI format are convenient to use and analyze since almost all the fMRI image software supports this kind of image. There is a widely used tool named dcm2nii, which has been developed by

Chris Rorden. It can automatically transform the DICOM file into a NIFTI file. In this study, the dcm2nii is used in the preprocessing command line.

4.1.2 Slice timing correction

The fMRI datasets are collected in two-dimensional images. Hence, the final three dimensional images are constructed slice by slice. But fMRI data is not collected in natural order, instead they are collected in a specific sequence, such as collecting odd ordered slices first, then collecting the even ordered slices. In order to eliminate those mismatches, a reference slice would be chosen. According to the reference slice, other slice will be interpolated to match the reference slice (Henson et al, 1999).

Nevertheless, if TR is less than 2 seconds, the error of slice mismatches can be tolerant for analysis.

4.1.3 Spatial Realignment

During the scanning, although subjects are instructed to be still and restrict head motion as much as possible, mostly there will be head motions anyhow since normal swallowing might cause a huge effect on the fMRI datasets. Even the most cooperative subjects would have a millimeter level's displacement (Russell et al., 2011). Basically, there are two kinds of effects of the head motion. The first one is the bulk motion, which means the whole brain is involved in the motion. For example, a head motion might cause certain voxels to change from no value to a certain value, and huge changes in these image intensities. Since all these kinds of changes only affect the spatial arrangement, the effect can be fixed by realigning the time series. Second, the motions can also distort the fMRI signal intensities (Friston et al., 1996b). Due to head motions, in some regions, several protons accidently move from their original slices to their neighboring slices.

After forming the image, intensities of voxels at those regions might not reflect the real activity intensity of matched brain tissue. This distortion would break the assumption that the fMRI signal describes the activities of real tissue at the specific brain. Worst of all, this kind of effect cannot be fixed by realignment. But it might be detected by independent component analysis (ICA).

The widely used and robust way to correct head motion is the realignment, which is one of the standard motion correction techniques. First, it estimates the 6 parameters of freedoms from the reference images. Then it uses these parameters to transform images to reach the maximized affinity of the reference image. Commonly, the mean image is used as the reference image.

There are several methods to interpolate through the transforming. The common and fastest way is linear interpolation, which mostly refers to the tri-linear interpolation. It takes the value weighed by those values around. But the linear interpolation might blur the image. Another way to interpolate is high-order interpolation, which provides a more accurate interpolation. It uses the Sinc function to replace the intensity of each voxel. The Sinc function is defined as:

$$Sinc(x) = \frac{\sin(x)}{x} \tag{4.1}$$

The interpolation values are calculated by summing the values from all other Sinc functions. In order to make the Sinc function interpolation more feasible, Hanning and rectangular windows can be used to choose the counted voxels.

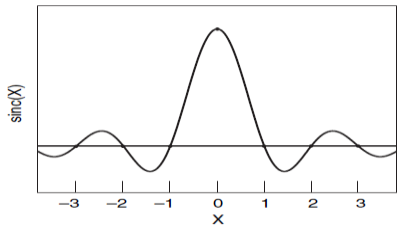

Figure 4.2 Sinc function

Source: Poldrack RA, Mumford JA, Nichols TE. (2011). Handbook of fMRI data analysis. New York, Cambridge University Press.

In addition to the Sinc, there are spline interpolation, which is mixed with nearest value interpolation and linear interpolation as well as non-linear interpolation. But the differences between those high-order interpolations are small (Oakes et al., 2005).

The reference image that the motion correction uses can be the mean image of the time series or just a specific one-time image. It seems that using the mean image may have no more benefit than using a signal time image since the mean image requires extra computation, and the mean image might be blurred after averaging. Thus it is better to choose one single time point image in the middle of the time series as reference image rather than the mean image.

Nevertheless, even with a perfect realignment, mostly movement-related signals may still exist. Hence, further steps are required to remove the residual movement related effects (Friston et al., 1996a). The reason that the residual movement still persists is that the linear derivative model cannot estimate the nonlinear effect. According to former papers, this nonlinear movement or displacement is originated from the listed resources: the interpolation artifacts (Grootoonk et al., 2000), which are attributed to interpolation errors from the resampling within the realignment; the shift of protons cause intensity changes, which is called spin-excitation history effects; the nonlinear distortion caused by

magnetic field inhomogeneity. These effects yield the nonlinear effect on the movement related signals (Friston et al., 1996a). Through using the estimated movement parameters and time series from realignment, the linear sum of a second order polynomial can estimate a function of movement, and then subtract these components which are correlated with the function of movement. It might remove all the artifacts as much as possible. But this subtraction might remove some information which is not artificial but real activations.

4.1.4 Spatial Smoothing

Generally, spatial smoothing is necessary for preprocessing the datasets. Although spatial smoothing might remove some high-frequency information, there are several reasons to do it. First, it can increase the signal to noise ratio for voxels. In addition, it can eliminate some effects from artifacts and make the errors more normal in their distribution. Second, blurring the data may decrease the spatial resolution, but it can reduce the difference between different subjects, which is fairly important for the group analysis. Third, some methods may require a specific degree of spatial smoothness. However, in some cases, spatial smoothing is forbidden since some algorithms , such as fALFF, are very sensitive to smoothing.

The most vital part of the smoothing is to find the balance between improving the signal to noise ratio yet maintaining the quality of the functional image. The common method to smooth the dataset uses the Gaussian kernel to convolute the three-dimensional images. The Gaussian function is showed below:

$$f(x,y,z) = \exp\left\{-\left(\frac{x^2}{2s_x^2} + \frac{y^2}{2s_y^2} + \frac{z^2}{2s_z^2}\right)\right\} \quad (4.1)$$

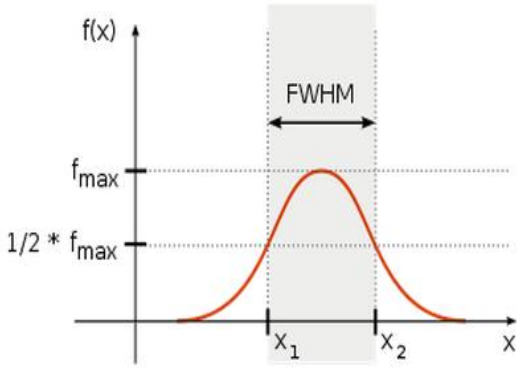

Figure 4.3 Smoothing function

Source: Poldrack RA, Mumford JA, Nichols TE. (2011). Handbook of fMRI data analysis. New York, Cambridge University Press.

The S_x, S_y and S_z represent the deviation of the Gaussian distribution in three directions. The width of the distribution determines the extent of the smoothing , and is described by the full width at half-maximum (FWHM) as the Figure 4.3 show. The mathematical relationship between the standard deviation and FWHM is $FWHM = 2\sigma\sqrt{2\ln(2)}$, nearly $2.55*\sigma$, in this study. For example the image of resolution is $2 * 3 * 4\text{mm}^3$, smoothing it with a 6mm FWHM Gaussian kernel. The sx, sy, sz should be:

$$Sx = \frac{6}{2.35 \times 2} = 1.27$$

$$Sy = \frac{6}{2.35 \times 3} = 0.85$$

$$Sz = \frac{4}{2.35 \times 4} = 0.42$$

Principally, the level of smoothing largely depends on the purpose of later analysis. In general, it is appropriate to choose the FWHM of smoothing ranging from 4 to 10 mm.

4.1.5 Spatial Normalization

In order to get a broad view on brain region or structure, the individual subjects have to be compared across each other. Since human brains vary in size and shape, it is obliged to transform all these subjects into a standard map. The process of how to transform these subjects is defined as spatial normalization or cross registration.

Two kinds of templates can be used for spatial normalization. The Talairach atlas, which was created by Talairach in 1967, is the most famous one. The full Talairach grid is based on several anatomical landmarks: the posterior commissure (PC), the anterior commissure, the middle sagittal plane, and the exterior boundaries. Thus, it is a kind of landmark-based normalization. However, the commonly used template is the one developed by the Montreal Neurological Institute, called the MNI template.

Here is the figure of how spatial normalization works:

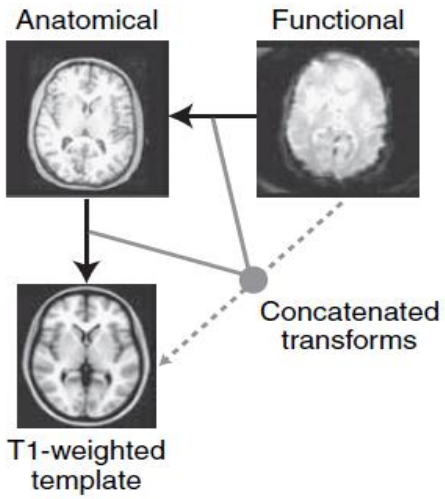

Figure 4.4 The spatial normalization process

Source: Poldrack RA, Mumford JA, Nichols TE. (2011). Handbook of fMRI data analysis. New York, Cambridge University Press.

First, the functional image is transformed to the anatomical image. The process also generates the first matrix of the transformation. Then the anatomical image is transformed into T1-weighted template with the second transformation matrix. The final transformation matrix can be created by concatenating the first and the second matrix. Eventually, by using the concatenated matrix, the functional image was transformed into the T1-weighted template. Therefore, these transformed functional images are in the standard images, and then can be used for group analysis. Basically, spatial normalization up samples the functional images, and increases the resolution of images. However, generally, there is no perfect correspondence between the anatomical image and the MNI template. Hence, a certain level of distortions might exit in the transformed functional images.

CHAPTER 5

fMRI ANALYSIS METHODS

5.1 Amplitude of Low Frequency Fluctuation

As mentioned in chapter 3, according to the study of Biswal and colleagues (Biswal et al., 1995), the synchronous low frequency fluctuation (LFF) in resting- state fMRI has highly correlated activities among the motor cortexes. In order to estimate the strength of the LFF, a parameter called the Amplitude of low frequency fluctuation (ALFF) was implemented by Zang in 2007.

Indeed, the way to calculate the Amplitude of low frequency fluctuation (ALFF) is coherent and simple (Zang, et al., 2007).The time series of each voxel in resting-state fMRI image was transformed to the frequency spectrum by the fast Fourier transform with the shortest points, and then the power spectrum is obtained by absolute value of the frequency spectrum. The amplitude of power spectrum at each frequency component is obtained by the square root of dividing the absolute value by the time points. Simply, ALFF is the sum of these amplitudes across 0.01 to 0.08Hz. Here is the equation:

$$ALFF = \sum_{k=a}^{b} \frac{|c_k|}{\sqrt{N}}, \tag{5.1}$$

$|C_k|$ is the amplitude of each frequency. ‘k’ refers to the frequency range, where ‘a’ and ‘b’ correspond to 0.01 and 0.08 Hz, respectively. N is the number of frequency points in the frequency spectrum. Fractional ALFF is calculated by dividing the ALFF by the sum of all the frequency components (Zhou et al., 2008). Here is the equation:

$$fALFF = \left\{ \sum_{k=a}^{b} \frac{|c_k|}{\sqrt{N}} \right\} \left\{ \sum_{k=0}^{N-1} \frac{|c_k|}{\sqrt{N}} \right\}^{-1} \quad (5.2)$$

5.2 Regional Homogeneity

Regional homogeneity (ReHo) (Zang et al., 2004) assumes that a given voxel is temporally similar to that of its neighbors. Regional homogeneity measures the similarity between the given voxel and its nearest neighbors on time series. Kendall's coefficient concordance (KCC) is used to calculate the ReHo.

Basically, ReHo is a complementary model-driven method, and it could help reveal the homogeneity of the human brain. The way that KCC (Kendall et al., 1990) is calculated shows below:

$$W = \frac{\Sigma(R_i)^2 - n(\overline{R})^2}{\frac{1}{12}K^2(n^3 - n)} \quad (5.3)$$

Where W is the KCC among given voxels, ranged from 0 to 1; R_i is the sum rank of the ith time point; $\bar{R}$ is the mean of the R_is; K is the number of time series within a measured cluster. For example, k could equal to 7, 19, and 27. The n is the number of time points (here, n=240).

5.3 Independent Component Analysis

Independent component analysis (ICA) is one of the blind source separation tools, which separates signal into independent signals based on certain feature of the signal. Here is a brief introduction of Independent component analysis (ICA) (Hyvarinen et al., 1997). Firstly, the independent components are defined. X is the observed signals, the S are the

source signals or independent components through ICA obtained. 'A' is the weighted matrix, which marks the "weight" of each component.

$$X = AS \tag{5.4}$$

In the ICA model, we assume that each mixture X_j and each independent component S_n is a random variable. The aj is one component of A, and X_j is one component of X. Thus the mixing model can be written as:

$$X_j = a_{j1}s_1 + a_{j2}s_2 + \ldots + a_{jn}s_n \text{ , for all j} \tag{5.5}$$

The very goal of the ICA is to find S, through observing X. By estimating the matrix A, and computing the inverse A, say W, it is easy to obtain S, these source components:

$$S = WX \tag{5.6}$$

According to the Central Limit Theorem (CLT), the distribution of the sum of independent random variables tends to be a Gaussian. Also CLT can be stated that the sum of two or more independent random variables usually has a distribution that is closer to Gaussian than either of each single variable. Finding the W, the weighted vector, is very important to solve the equation (2). Thus maximizing the non-gaussianity of WX can be used as a way to obtain the independent components. There are several ways to estimate the non-gaussianity of WX. Non-gaussianity is measured by the approximation of negentropy $J(W^T X)$:

$$J(y) \approx \frac{1}{12} E\{y^3\}^2 + \frac{1}{48} Kurt(y)^2 \tag{5.7}$$

The most popular way is the Fast ICA. These are some basic steps of Fast ICA. First, before working on the data, there are two steps of pre-processing, which include centering and whitening. What centering usually does is to subtract its mean m =E{x}. It

can make x a zero-mean variable. Whitening the data almost makes the components uncorrelated and its variance unity. Then ICA starts with

Step 1: choose an initial weight vector W;

Step 2: Let w= $E\{xg(w^Tx)\}-E\{g`(w^Tx)\}$ w ; g(u)=tanh(u);

Step 3: Let w=w+/|w+|;

Step 4: If w is not converged, go back to step 2.

The maximum of the approximation of negentropy of WX is obtained by step 2. Through the loop (step2 to step 4), the best W matrix for these data will be obtained.

In this experiment, in order to find the feature of BOLD signals in the infarct and penumbra, spatial ICA (Peterson et al., 2000) is used to separate the infarct or penumbra regions out of normal regions, since the BOLD signals in the infarct or penumbra regions might be independent of these BOLD signals in other regions . In the spatial ICA, X is a flattened fMRI data, which is an N-by-M matrix. N equals to the number of time points, and M equals to the number of voxels. X is the separated individual sources, which is the spatially independent components in this study. Figure 5.1 illustrates the corresponding X, W, S respectively, in this study.

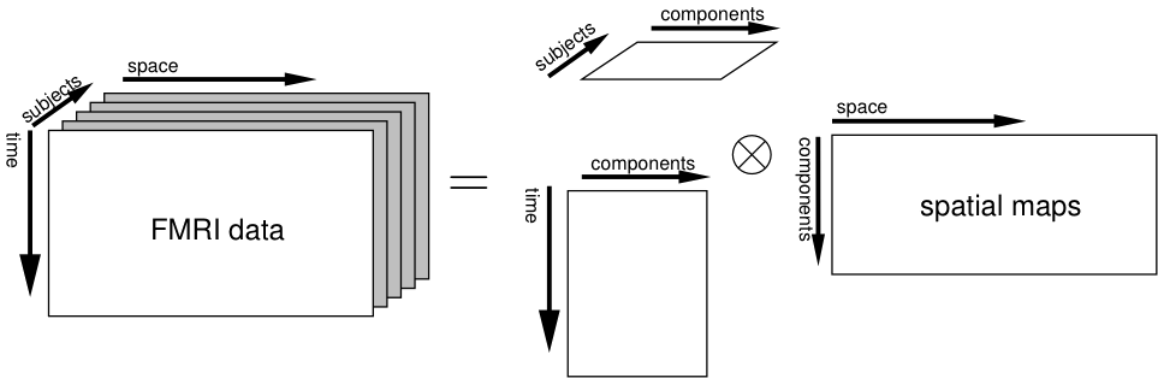

Figure 5.1 Spatial ICA on multi-session fMRI

Source: http://www.fmrib.ox.ac.uk, accessed on May 14, 2012

The FSL software package is chosen to calculate the spatial ICA. Usually, the output components are set to 40 components, which in the most cases reach to the 0.95% of all possibility. After the ICA, the results are flattened spatial maps, which need to be reshaped into 3 dimension matrixes to present brain structures.

CHAPTER 6

fMRI FINDINGS

As a widely used and non-invasive tool, functional magnetic resonance imaging (fMRI) provides a unique setting to study the human brain. Compared to diffusion weighted imaging, fMRI has a lower spatial resolution but its temporal dimension can provide information on the dynamics of the brain activities. The basic goal of this study is to obtain both structural and functional information about lesions in stroke patients. Those methods that were described in Chapter 5 are summarized below:

6.1 Methods Review

I. Basic statistical parameters for time series. We calculate the standard deviation for time series at each voxel. The standard deviation may demonstrate different levels of variants from the averages of the fluctuation in the infarct regions and in the penumbra regions. Moreover, the mean of each voxels is counted. This parameter might provide the information about the baseline of neuron activities at different regions.

II. ALFF and fALFF focus on the fluctuation amplitude in the low frequency ranging from 0.01 to 0.08 Hz. According to the assumption that neuron activities in the infarct regions might decline, the ALFF and fALFF values at the infarct regions would be expected to decrease synchronously.

III. Regional Homogeneity (ReHo) measures the temporal similarity of adjacent voxels. The prediction for the result of this method is that the synchrony of

local voxels in the lesion brain regions will be lower than in other normal brain regions.

IV. Spatial independent component analysis (ICA) is generally used to separate spatially independent brain regions which have similar activity patterns. If the BOLD signals in the infarct regions and in the penumbra regions are altered and dissociated with other brain regions, a separate independent component of the infarct and penumbra regions would be expected.

In this study, the result of all methods will be presented, including ALFF, fALFF, ReHo, the mean of each voxel, and the standard deviation of each voxel.

6.2 EPI Images after Preprocessed Steps

Figure 6.1 below presents the preprocessed images of a normal control group and an ischemic stroke group. Compared with the normal control group, those subjects in the ischemic stroke group have a bigger shape of Cerebrospinal fluid (CSF). The explanation might be that subjects in the ischemic stroke group are older people, or those subjects also may have certain levels of hydrocephalic symptoms. Subject 12 in the ischemic stroke group shows the lesion in the inferior occipital gyrus. The Black hole indicated that there is no BOLD signal, and the tissues might be totally dead.

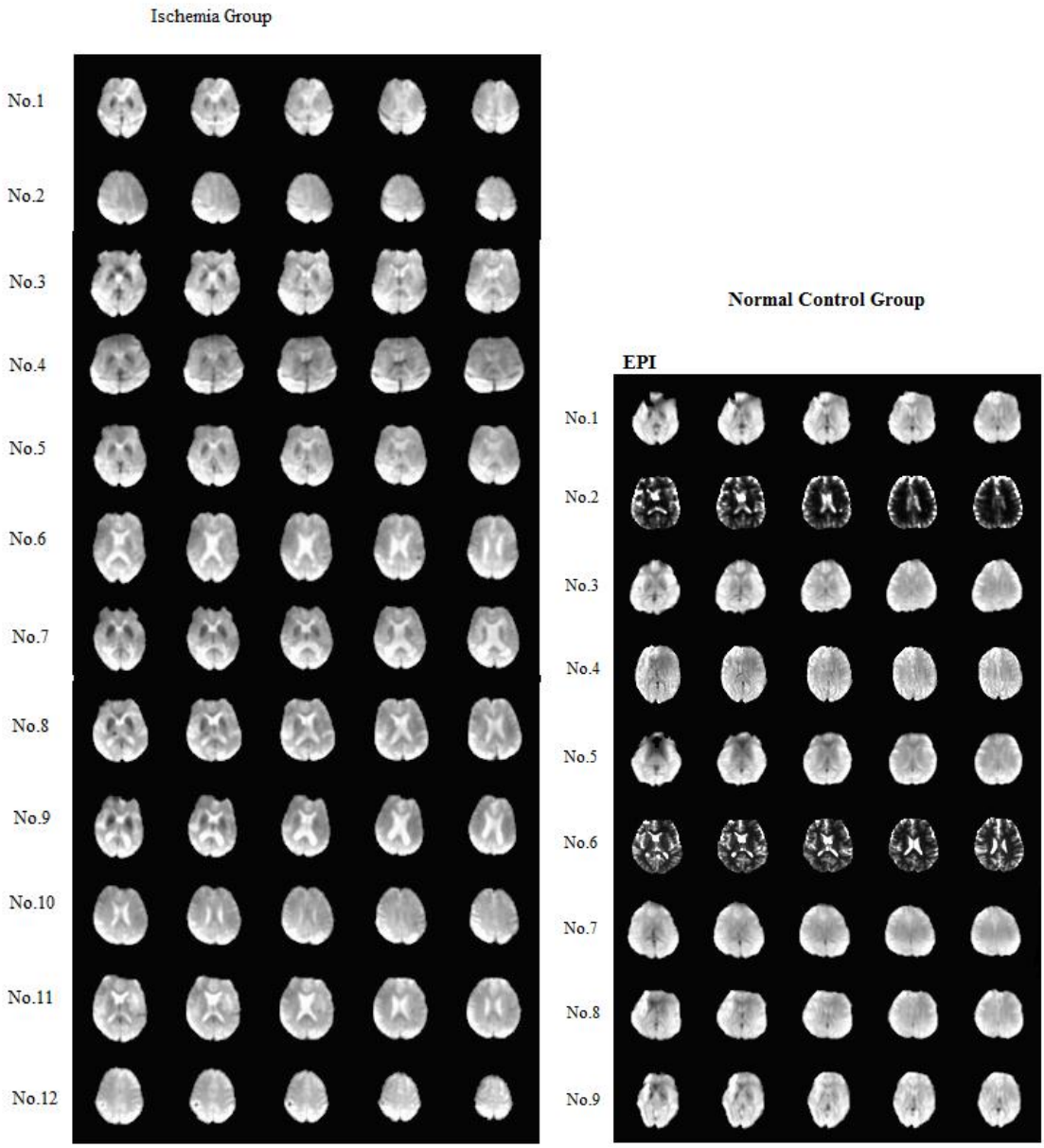

Figure 6.1 The EPI image of subjects in normal control group and ischemic group

6.3 Analysis of Normal Control Group

In order to compare the brain image in the normal control group with those in the ischemic stroke group, all the subjects in the normal control group are analyzed in the

same way as those in the ischemic group. As figure 6.2 shows, those normal subjects usually have a symmetrical structure.

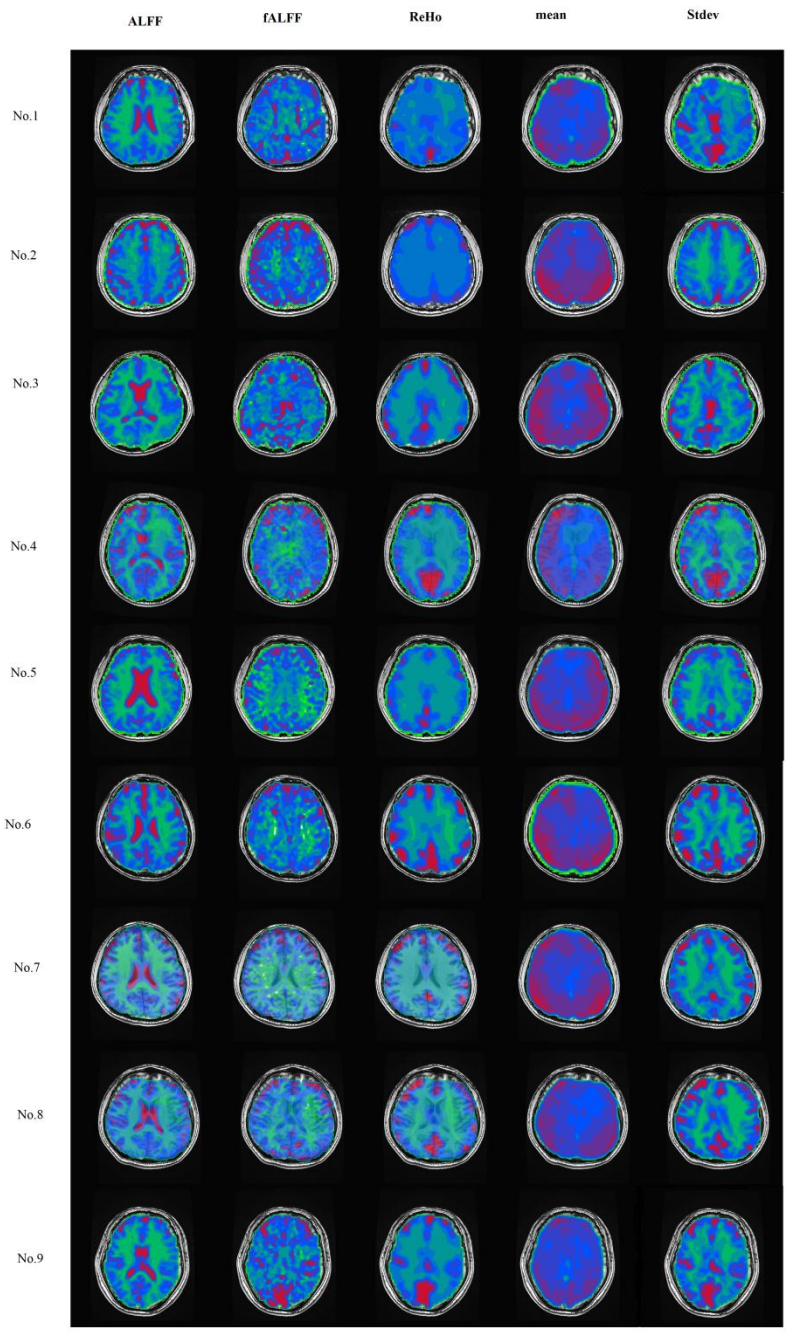

Figure 6.2 ALFF, fALFF, ReHo and standard deviation result of Normal control group

6.3.1 Time Series and Frequency Spectrums

According to the previous study (Biswal et al, 1995), the signal with frequency ranging from 0.01 to 0.08 Hz is highly correlated with neuron activities. In fact, there are several physiologic sources in the BOLD signal. For example, the respiratory rate noise and heart rate noise are the main noise sources in the resting state fMRI. The time series is shown below.

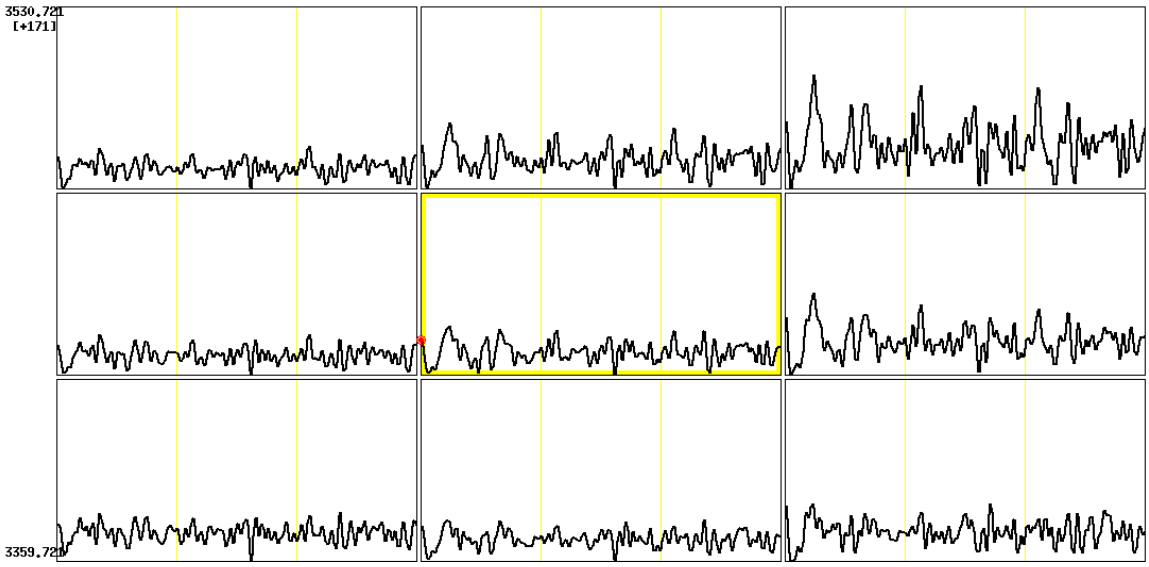

Figure 6.3 Time series from normal subject

The frequency spectrum:

Figure 6.4 shows the frequency spectrum in the raw data. Since the TR equals to 2.0s, the highest frequency component is 0.25Hz. The figure shows that frequency components lower than 0.1Hz have higher amplitudes than those higher frequency components.

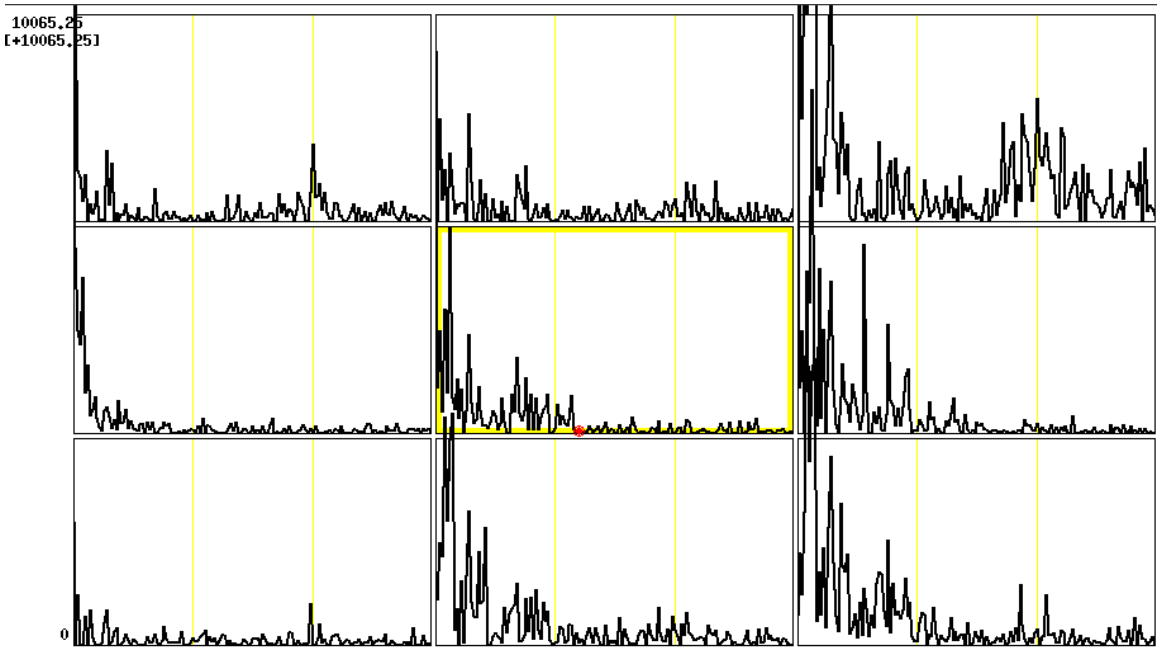

Figure 6.4 Frequency spectra without filtering

The frequency spectrum after the band pass filter:

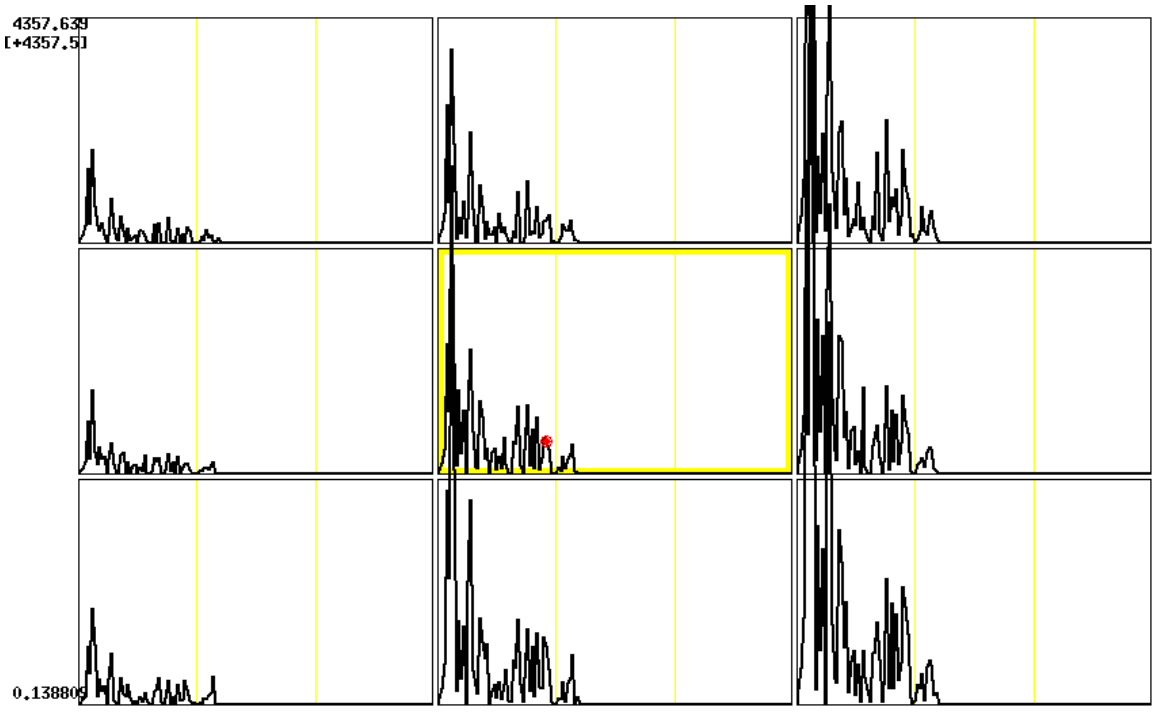

Figure 6.5 Frequency spectra with filtering

6.4 Analysis of the Ischemia Group

Just as same as the normal group, Subjects in the ischemia group are analyzed by ALFF, fALFF, ReHo and standard deviation. Figure 6.3 demonstrates the analysis results of the subject 11:

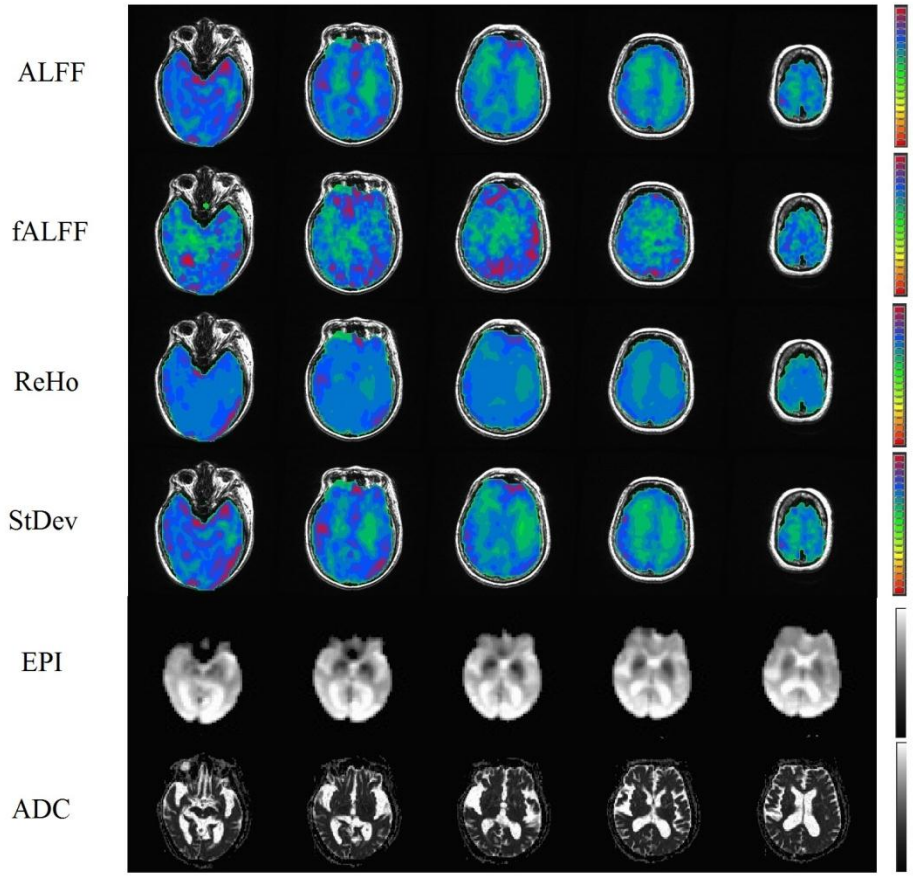

Figure 6.6 Analysis results of subject 11

As the reference image ADC shows, on the right side of the image or the left side of brain, there is a lesion at the temporal lobe. Although the position and the size of the lesion that ALFF and ReHo indicate are not the same as it shown in the ADC, the huge difference between the ALFF and ReHo between the left side and the right side of brain can tell that ischemic stroke affects the BOLD signal on the time domain and frequency domain.

The subject 12 is:

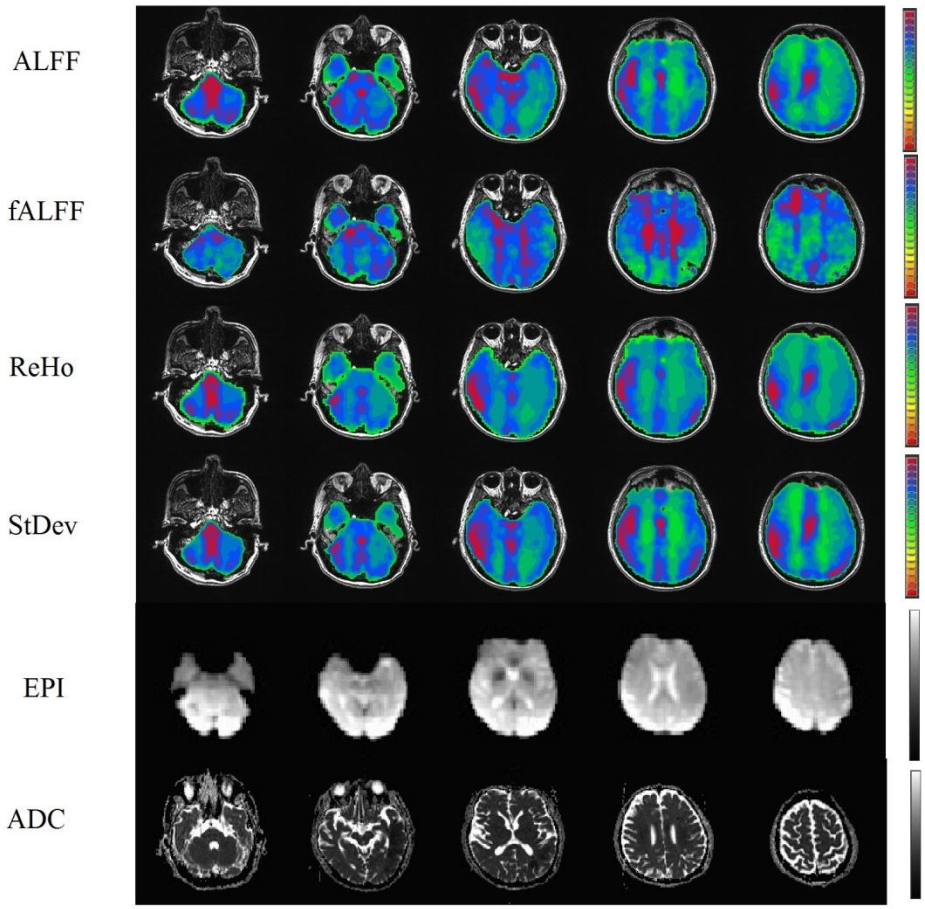

Figure 6.7 Analysis results of subject 12

According to the second ADC map, the lesion is around left frontal lobe, which on the right side of these images since the medical image is reversed. As the ALFF, ReHo show, the left side of the brain has low values than the right side. Although the location of lesion might not match perfectly, the basic difference is clear.

The subject 13:

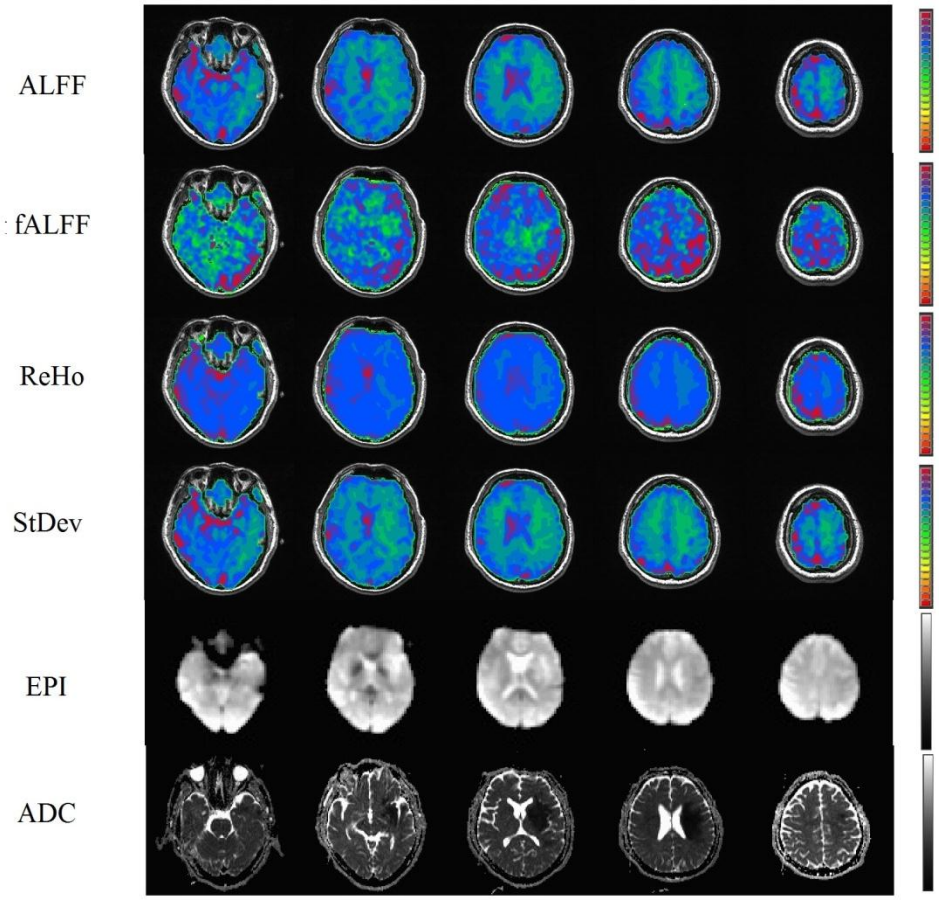

Figure 6.8 Analysis results of subject 13

As these three subjects present, ALFF and ReHo, standard deviation can show the difference between the lesion and normal tissue. But it is far from being able to distinguish the infarct and penumbra. Even at the same brain region, each subject has dramatically different values. In order to compare the changes of ALFF in infarct and penumbra across subjects, values from contralateral health tissues in each subject are measured to normalize the infarct and penumbra value.

For each subjects, we drew ROI masks for infarct regions, penumbra regions and normal regions, then average these values. In the table 6.1, 1st column to 7th column are these results. Since some subjects have very small infarct, which technically cannot draw

a mask on it, values randomly are picked up inside infarct instead. For those subjects who have no penumbra regions, zeros are used to present.

Table 6.1 ALFF value of different regions from each subject

	1	2	3	4	5	6	7	8	9
	infarct	penumbra	normal	n_infarct	n_penumbra	n_n	infarct/normal	penumbra/normal	normal/n_n
1	68603.33857	76446.9125	82642.31	73445.569	80252.56375	85476.03063	0.830123681	0.925033588	0.966847775
2	63805.27889	121034.93	129714.2714	84799.97	84897.75286	118974.7429	0.491890971	0.93308877	1.090267298
3	23647.01889	0	30201.94125	28660.55231	0	25011.162	0.782963542	0	1.207538508
4	99192.56444	146215.6375	109484.3117	115507.553	108313.5167	112578.5233	0.905997973	1.335493965	0.97251508
5	42996.38	0	29443.23667	26176.375	0	27217.035	1.460314316	0	1.081794423
6	18635.92667	0	32429.765	19232.91667	0	20615.374	0.574655002	0	1.573086426
7	29668.22333	35988.186	29737.765	25653.53167	27245.908	26825.17833	0.997661503	1.210184626	1.1085766
9	21419.85333	22069.81545	29081.75	25244.33	28616.48375	20037.96286	0.736539353	0.758888838	1.451332663
11	31947.00778	38972.835	44171.03833	42689.63556	47085.47	42799.61	0.723256889	0.882316479	1.03204301
12	186710.2125	149857.5625	121987.3567	164524.64	123175.15	176871.8143	1.530570197	1.228467987	0.689693591
13	24591.09111	32917.38364	30914.77333	30509.81778	40640.33667	30877.48222	0.795447887	1.064778424	1.001207712
14	14809.75	0	15678.59909	16189.69818	0	17150.19	0.944583755	0	0.914193901
15	30790.63333	38780.67667	30667.04167	28559.62667	37279.166	25380.49375	1.004030114	1.264571819	1.208291768
average							0.906002706	1.066980499	1.099799135

In this table, “normal” means the normal region at the side of the brain with infarct. “n_n” means the normal region at the contralateral side of the brain with infarct. Thus, in the table, “n_” means contralateral. In order to confirm the difference between the penumbra regions and normal regions, the t-test is used, and p values are recorded as table 6.2.

Table 6.2 T-test on penumbra and normal regions

group	penumbra|n_penu	penumbra|normal	(penumbra/n)|(normal/n_n)
p value	0.088592309	0.150026167	0.109069048

As the 7th column of the table shows, the majorities of ratios between the infarcts and contralateral normal tissues are lower than 1. Because cells in the infarct are in the destruction process and basically those cells have no neuron activities. Thus, BOLD signal at these regions might have low fluctuation. Hence, compared with normal tissue, ALLF of infarct is low. For cells in penumbra, their ALFF values changes dramatically across subjects. As the 8th column shows, radios are not strictly higher than 1 or lower than 1. These various penumbra ratios are closer to the fact that condition of cells in penumbra region changes through times. At the onset time, the collateral effect might increase the fluctuation of BOLD signal as well as increasing the ALFF values. When the

blood flow keeps on dropping, cells start to deconstruct, the fluctuation of BOLD signals drop and the ALFF decreases.

As previous chapter introduced, ICA is a data based method, which can be uses under the assumption that the signal which is highly correlated to the infarct, and penumbra is independent to other signals. In this study, these features of BOLD signal in infarct and penumbra make it reasonable to try the ICA.

As the Figure 6.6 shows, the ADC image below indicates the infarct of the brain. The numbers of these brain axial slices are from 15 to 19 (there are 36 axial brain slices). The red part of the brain shows lowest level of water diffusion, which is a clear inference that these brain tissues may lose its biological activation. Basically, these red regions inside brain can be defined as infarct.

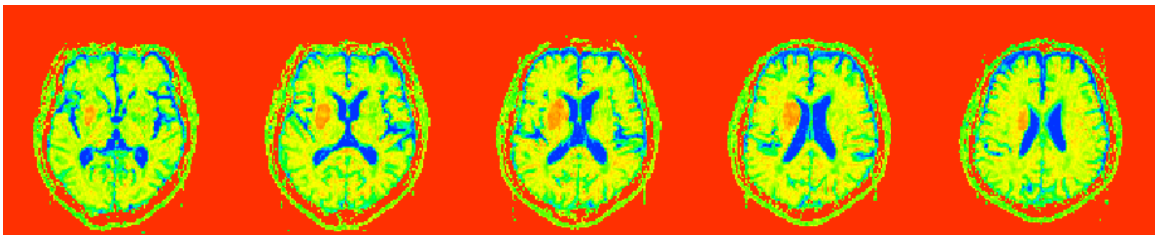

Figure 6.9 ADC of subject 3 in color

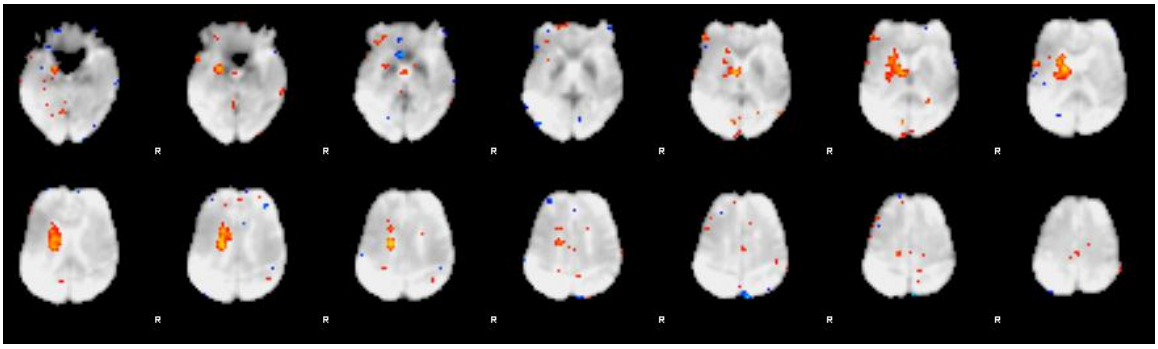

Figure 6.10 ICA result (one independent component)

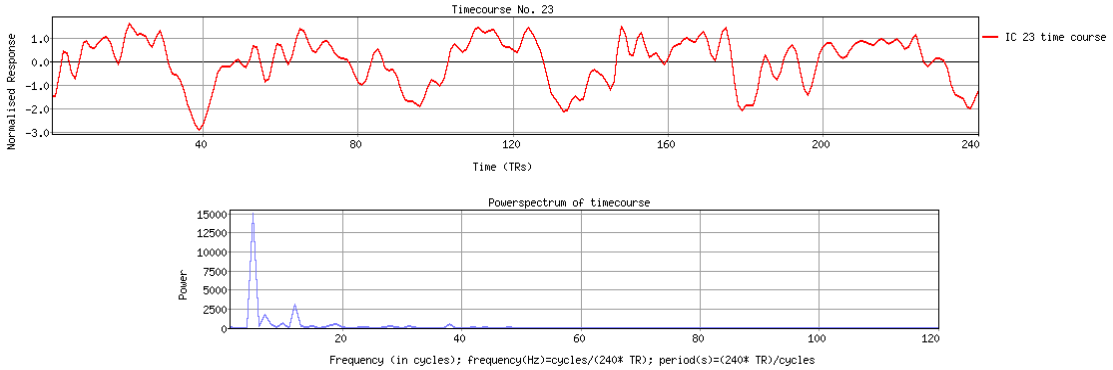

Figure 6.11 Time series and frequency spectrum of this component

The ICA result perfectly matches with the ADC map. The frequency spectrum shows that the frequency around 0.03HZ is the main frequency in the signal of the infarct region.

CHAPTER 7

CONCLUSION AND FUTURE STUDY

The diffusion weighted image can detect lesions fast and accurately. fMRI might provide more information on the relationship between the structure and function of lesions. As the results demonstrate, ALFF, fALFF and ReHo cannot accurately present the infarct region. But they provide several interesting features of the BOLD signal at those regions. First, it was found that the focal ischemic infarct would cause a decrease in ALFF since contralateral normal regions have higher ALFF values. The reason might be that since tissue in the infarct is on the destruction process and the blood supply is extremely lower than normal, the fluctuation of the BOLD signal would decrease. When the fluctuation of BOLD signal decreases, the standard deviation decreases. According to the previous study, LFF is mostly related to neuron activities but not physiological effects. For these cells in the infarct region, both neuronal related activities and physiological activities are decline dramatically. For the penumbra region, all the analysis methods show that the values in penumbra part are not consistently higher or lower than those in the normal tissue across each subject. It might because that at different time phases, the status of the tissue in the penumbra is changing over time. Due to the smaller sample amount, the result might be invalid. It is difficult to build a correlation with the penumbra over normal tissue ratio and time. Moreover, in the practical study, there are several physiological noises coupled with the BOLD signal, such as cardiac rate, respiratory rate, and vasomotor. Even with an extremely strict filter or regression method, those kinds of noise

residues are still inside the signal. Thus, ALFF might present neuronal activities as well as some physiological changes.

The results also demonstrate that differences between infarct and penumbra can be detected in some cases, such as subject 13. However, this kind of difference is not huge and clear enough to figure out specific changes in the BOLD signal as well as to distinguish the infarct and penumbra. Moreover, the t-test result demonstrates that there is no significant difference between the infarct regions and bilateral normal regions as well as penumbra regions and its bilateral normal regions. The reason might be categorized into three parts. One is the signal source itself. Multiple sources inside the BOLD signal increase the complex of analyzing one single effect. Second, different subjects might have different physiological conditions. For example, some subjects may have higher tolerance to ischemia than others. Thus, those subjects would have lower physiological changes than others. Moreover, even for one subject, at a different ischemic stage, there are various and dramatic changes on BOLD signal. The third reason is the relatively small sample volume. There are fifteen subjects and one out of three have no penumbra region. Considering the factors that have to take into account, this amount of subjects are not enough.

In conclusion, in some cases, ALFF and ReHo can show an apparent contrast between infarct and bilateral normal regions as well as in the penumbra and its bilateral regions. But according to the t-test (Table 6.2), there is no significant difference of ALFF and ReHo between infarct and normal regions or between penumbra and bilateral regions across subjects. It might because subjects are scanned at different times, and the tissues in the infarct and penumbra change through time. The component of the BOLD signal

which is related to neuronal activities might decrease; however, some components of the BOLD signal which originate from other physiological sources might increase. Thus the BOLD signal changes in the infarct and penumbra vary, but not monotonically decrease, or monotonically increase. Hence, ALFF or ReHo cannot present a good contrast between lesions and bilateral regions in every subject. By increasing the sample volumes, probably, a clear correlation between the time period of stroke and the changes of BOLD signals in lesions might be achieved.

Nevertheless, it does not mean that there is no possibility to find some specific BOLD signal features in the infarct and penumbra. Indeed, there are some inspiring ideas about the future work. For ALFF and fALFF, it is reasonable to narrow down the frequency range and examining each short-band frequency component. Definitely, it takes a great deal of time to do. But according to the result, it might be the final solution. For the ICA, increasing independent components could be a solution. Since the 40 components result indicated too much noise, increasing the independent components probably could increase the chance to detect the lesions.

REFERENCES

Anand, A., Li, Y., Wang, Y., Wu, J., Gao, S., Bukhari, L., Mathews, V.P.,Kalnin, A., Lowe, M.J. (2005). Activity and connectivity of brain mood regulating circuit in depression: a functional magnetic resonance study. Biol. Psychiatry 57, 1079–1088.

Blank-Reid, C. (1996). How to have a stroke at an early age: The effects of crack, cocaine and other illicit drugs. Journal of Neuroscience Nursing. 28(1), 19–27.

Biswal, B., Yetkin, F.Z., Haughton, V.M., Hyde, J.S., (1995). Functional connectivity in the motor cortex of resting human brain using echo-planar MRI. Magn Reson Med. 34, 537–541.

Chen PE, Simon JE, Hill MD. (2006). Acute Ischemic Stroke: Accuracy of Diffusion-weighted MR Imaging—Effects of b Value and Cerebrospinal Fluid Suppression Radiology, pp. 232–239

Cordes, D., Haughton, V.M., Arfanakis, K., Carew, J.D., Turski. (2001). Frequencies contributing to functional connectivity in the cerebral cortex in "restingstate" data. Am. J. Neuroradiol. 22, 1326–1333.

Cox, R.W. (1996). AFNI: software for analysis and visualization of functional magnetic resonance neuroimages. Comput. Biomed. Res. 29, 162–173.

Dagli,M.S, Ingeholm, J.E, and Haxby,J.V. (1999).Localization of cardiac-induced signal change in fMRI, Neuroimage, 407–415.

Friston, K. J., Ashburner, J., Frith, C. D., Poline, J.-B., Heather, J. D., and Frackowiak, R. S. J. (1995). Spatial registration and normalization of images. Brain Mapp, 2, 165–189.

Friston, K. J., Williams, S., Howard, R., Frackowiak, R. S. J., and Turner, R. (1996). Movement-related effects in fMRI time-series. Magn. Reson. Med, 35, 346–355.

Fox,M.D.,and Raichle,M.E. (2007). Spontaneous fluctuations in brain activity observed with functional magnetic resonance imaging. Nat. Rev. Neurosci, 8,700–711.

Greicius, M.D., Srivastava, G., Reiss, A.L., Menon, V. (2004). Default-mode network activity distinguishes Alzheimer's disease from healthy aging: evidence from functional MRI. Proc. Natl. Acad. Sci. U. S. A. 101, 4637–4642.

Goldstein M, Barnett HJ, Orgogozo JM, et al. Stroke. (1989). Recommendations on stroke prevention, diagnosis, and therapy. Report of the WHO Task Force on Stroke and other Cerebrovascular Disorders. Stroke, 20, 1407-1431.

Grootoonk, S., Hutton, C., Ashburner, J., Howseman, A. M., Josephs, O., Rees, G., Friston, K. J., and Turner, R. (2000). Characterization and correction of

interpolation effects in the realignment of fMRI time series. NeuroImage, 11, 49–57.

Goetz CG, Pappert EJ. (1999). Textbook of Clinical Neurology. 1st ed. Philadelphia, Penn: WB Saunders Company, 373, 917.

Hickey, J. V. (2003). The clinical practice of neurological and neurosurgical nursing (5th ed.). Philadelphia: Lippincott, Williams & Wilkins.

Hinkle JL, Guanci MM. (2007)Acute ischemic stroke review. J Neurosc Nurs, 39, 285-293.

H. Yang, X.Y. Long, Y.H. Yang, H. Yan, C.Z. Zhu, X.P. Zhou et al. (2007). Amplitude of low frequency fluctuation within visual areas revealed by resting-state functional MRINeuroImage, 36, 144–152

Hyvarinen, A. and Oja, E. (1997). A fast fixed-point algorithm for independent component analysis. ¨ Neural Computation, 9(7), 1483–1492.

Jo,H.J, Saad, Simmons, W.K, Milbury, L.A, and R.W.Cox. (2010). Mapping sources of corre-lation inresting state FMRI, with artifact detection and removal. Neuroimage 52, 571–582.

Jones TH, Morawetz RB, Crowell RM, et al. (1981). Thresholds of focal cerebral ischemia in awake monkeys. J Neurosurg, 54, 773-782.

James R. Carey, Teresa J. Kimberley, Scott M. Lewis. (2002). Analysis of fMRI and finger tracking training in subjects with chronic stroke. Brain 125 (4), 773-788.

Joshipura, K. J., Hung, H., Rimm, E., Willett, W., & Ascherio, A. (2003). Periodontal disease, tooth loss, and incidence of ischemic stroke. Stroke, 34(1), 47–52.

Kendall, M., Gibbons, J.D. (1990). Rank Correlation Methods. Fifth edition, New York: Oxford University Press.

Kiviniemi, V., Kantola, J.H., Jauhiainen, J., Tervonen, O. (2004). Comparison of methods for detecting nondeterministic BOLD fluctuation in fMRI. Magn. Reson. Imaging 22, 197–203.

Lange, N., Zeger, S.L. (1997). Non-linear fourier time series analysis forhuman brain mapping by functional magnetic resonance imaging. J. R.Stat. Soc. Appl. Stat. 46, 1–29.

Le Bihan D, Breton E, Lallemand D, Grenier P, Cabanis E, Laval-Jeantet M. (1986) MR imaging of intravoxel incoherent motions: application to diffusion and perfusion in neurologic disorders. Radiology, 161, 401-407.

Li, S.J., Li, Z., Wu, G., Zhang, M.J., Franczak, M., Antuono, P.G. (2002). Alzheimer disease: evaluation of a functional MR imaging index as a marker. Radiology 225, 253–259.

Lowe,M.J.,Mock,B.J.,andSoren-son, J.A. (1998). Functional connectivity in single and multislice echo planar imaging using resting-state fluctuations. Neuroimage, 7,119–132.

Lutsep HL, Albers GW, DeCrespigny A, Kamat GN, Marks MP, Moseley ME. (1997). Clinical utility of diffusion-weighted magnetic resonance imaging in the assessment of ischemic stroke. Ann Neurol, 41, 574-580.

Maarten G. Lansberga, Vincent N. Thijsa, Michael W. O'Briena, Juan O. Alia, Alex J. de Crespignya, David C. Tonga, Michael E. Moseleya and Gregory W. Albersa. (2001). Evolution of Apparent Diffusion Coefficient, Diffusion-weighted, and T2-weighted Signal Intensity of Acute Stroke. AJNR 22, 637-644

Maas MB, Safdieh J. Ischemic Stroke: Pathophysiology and Principles of Stroke Localization. In: Atri A, Milligan T, editors. (2009). Hospital Physician Neurology Board Review Manual. Wayne, PA: Turner White Communications

Mullins ME, Schaefer PW, Sorensen AG, et al. (2002) CT and conventional and diffusion-weighted MR imaging in acute stroke: study in 691 patients at presentation to the emergency department. Radiology, 224, 353-360.

Oakes, T.R., Johnstone, T., Ores Walsh, K.S., Greischar, L.L., Alexander,A.L., Fox, A.S., Davidson, R.J., (2005). Comparison of fMRI motion correction software tools. NeuroImage 28 (3), 529–543.

Peterson KS, Hansen LK, Kolenda T, Rostrup E, and Strother SC. (2000). On the independent components of functional neuroimages. Proceedings ICA. Helsinki. Espoo, Finland: Otamedia.

Poldrack RA, Mumford JA, Nichols TE. (2011). Handbook of fMRI data analysis. New York, Cambridge University Press.

Qi-Hong Zou, Chao-Zhe Zhua, Yihong Yangb, Xi-Nian Zuoc, Xiang-Yu Longa. (2008). An improved approach to detection of amplitude of low-frequency fluctuation (ALFF) for resting-state fMRI: Fractional ALFF. Journal o Neuroscience methods, Volume 172, Issue 1, 137–141

Raichle, M.E., MacLeod, A.M.,Snyder, A.Z.,Powers,W.J., Gusnard, D.A.,and Shulman, G.L. (2001). A default mode of brain function. Proc. Natl. Acad. Sci. U.S.A. 98, 676–682.

Roy, A.K., Shehzad,Z., Margulies, D.S., Kelly,A.M., Uddin,L.Q., Gotimer, K., Biswal, B.B., Castellanos, F.X., and Milham, M.P. (2009). Functional connectivity of the human amygdala using resting state fMRI. Neuroimage 45, 614–626.

Van Everdingen KJ, van der Grond J, Kappelle LJ, Ramos LM, Mali WP. (1998). Diffusion-weighted magnetic resonance imaging in acute stroke. Stroke, 29, 1783-90.

Warach S, Chien D, Li W, Ronthal M, Edelman RR. (1992). Fast magnetic resonance diffusion-weighted imaging of acute human stroke. Neurology; 42(9), 1717–1723.

Ward N. S., M. M. Brown, A. J. Thompson and R. S. J. Frackowiak. (2003) Neural correlates of motor recovery after stroke: a longitudinal fMRI study. Brain 126 (11), 2476-2496.

Ward N. S., M. M. Brown, A. J. Thompson and R. S. J. Frackowiak. (2003) Neural correlates of outcome after stroke: a cross sectional fMRI study. Brain 126 (6), 1430-1448.

Wise, R.G, Ide, K, Poulin, M. J, and Tracey, I. (2004). Resting fluctuations in arterial carbon diox-ide induce significant low frequency variations in BOLD signal. Neuroimage 16, 52–64.

Woodhams R, Ramadan S, Stanwell P, Sakamoto S, Hata H, Ozaki M. (2011) Diffusion-weighted imaging of the breast: principles and clinical applications. Radiographics, 31, 1059–84.

Zang, Y., Jiang, T., Lu, Y., He, Y., & Tian, L. (2004) Regional homogeneity approach to fMRI data analysis. Neuroimage, 22, 394–400.